CrossMark

Microstructural Analysis and Transport Properties of Thermally Sprayed Multiple-Layer Ceramic Coatings

Hsin Wang[1] · Govindarajan Muralidharan[1] · Donovan N. Leonard[1] ·
J. Allen Haynes[1] · Wallace D. Porter[1] · Roger D. England[2] · Michael Hays[2] ·
Gopal Dwivedi[3] · Sanjay Sampath[3]

Abstract Multilayer, graded ceramic/metal coatings were prepared by an air plasma spray method on Ti-6Al-4V, 4140 steel and graphite substrates. The coatings were designed to provide thermal barriers for diesel engine pistons to operate at higher temperatures with improved thermal efficiency and cleaner emissions. A systematic, progressive variation in the mixture of yttria-stabilized zirconia and bondcoat alloys (NiCoCrAlYHfSi) was designed to provide better thermal expansion match with the substrate and to improve thermal shock resistance and cycle life. Heat transfer through the layers was evaluated by a flash diffusivity technique based on a model of one-dimensional heat flow. The aging effect of the as-sprayed coatings was captured during diffusivity measurements, which included one heating and cooling cycle. The hysteresis of thermal diffusivity due to aging was not observed after 100-h annealing at 800 °C. The measurements of coatings on substrate and freestanding coatings allowed the influence of interface resistance to be evaluated. The microstructure of the multilayer coating was examined using scanning electron microscope and electron probe microanalysis.

Keywords TBC · thermal barrier coatings · thermal diffusivity

✉ Hsin Wang
   wangh2@ornl.gov

1   Oak Ridge National Laboratory, Oak Ridge, TN 37831, USA

2   Cummins Inc., Columbus, IN, USA

3   SUNY Stony Brook, Stony Brook, NY, USA

Introduction

Ceramics coatings have long been used as thermal barriers for aircraft and automobile engines operating at high temperatures (Ref 1, 2). Thermal barrier coatings (TBCs) allow the engine gas temperatures to significantly exceed the limits of traditional alloys or steels, which benefits engine efficiency, and in some cases, emissions (Ref 3). Many studies have focused on lowering thermal conductivity of the coatings, while still maintaining good thermomechanical integrity (Ref 4, 5). Besides lowering thermal conductivity by doping heavy elements for phonon scattering, multiple-layer TBCs have been used to increase interface scattering of the phonons and oxidation resistance (Ref 5). For example, alternate YSZ and YAG layers were used to promote interface scattering (Ref 4).

Initial applications of TBCs on diesel engines were carried out using a Cummins V903 direct injection engine under DOE/NASA and TACOM programs (Ref 6) focusing on cylinder head and piston coatings. The TBC is designed as a thermal shield, with the goal of ultra-low thermal conductivity. However, this reduced thermal conductivity can also be a source of high thermal stresses, particularly in thicker coatings. Although TBCs have been used to protect internally cooled stationary and rotating hot section components in aero engines and land-based turbines for decades, introduction of TBCs into high-volume reciprocating engines has been a very slow process due to the extreme conditions on the piston crown surface and the very long service lives of heavy duty diesel engines prior to first overhaul (Ref 6-8). On the other hand, TBCs have been widely used in race car engines in which short-term performance is more important than long-term durability (Ref 9). Improving the thermomechanical properties of the TBC

🍦 Springer

system, while maintaining or improving thermal resistance, is a key for commercial TBC applications in diesel engines.

A typical TBC system for aircraft applications consists of an alloy (Ni-base super alloy) substrate coated with a bondcoat (MCrAlY) and then a ceramic top coating (e.g., 8YSZ). A thermally sprayed bondcoat provides oxidation resistance to the substrate and a roughened surface for mechanical bonding of the ceramic top coat and may also provide a buffer region to transition from alloy to ceramic thermal expansion behavior. However, there is still a clear boundary between the bondcoat and TBC which forms thermally grown oxides (TGO) due to oxidation of the bond coat during high temperature exposure. This oxidized interface is a major contributor to delamination failure of the ceramic top coat and remains a weak link for TBCs. The cyclic nature of piston strokes in a reciprocating engine adds high-frequency thermomechanical stresses to the coating. A simple substrate bondcoat TBC system will not typically survive these conditions to achieve long-term engine service life for commercial vehicles.

An improved approach is to utilize a functionally graded coating system with a gradual transition from bondcoat to ceramic coating in order to better accommodate and minimize thermal stresses (Ref 10-12). In the present study, a multiple-layer coating system was designed with four layers of mixed bondcoat alloy (NiCoCrAlYHfSi) and yttria-stabilized zirconia (YSZ). The graded alloy and YSZ mixture were intended to achieve a better match of thermal expansion coefficient (CTE) and minimize thermal stresses. In this study, we focus on the coating development on various substrates and report thermal transport properties of the multiple-layer system and its microstructure.

Experimental

Thermal barrier coatings were prepared at the Thermal Spray Laboratory at SUNY Stony Brook using an air plasma spray system. To evaluate thermal conductivity of various coating architectures, coatings were deposited on the flat surface cylinders of 12.7 mm diameter disks with 15 mm thickness. Three different substrate materials were selected for this study, Ti-6Al-4V, 4140 steel and graphite. Graphite was used to prepare freestanding coatings by grinding off the soft substrate material. In order to improve coating adhesion, the metal substrate surfaces were grit-blasted at a pressure of 4 bar using Al_2O_3 grit, which resulted in surface roughness of ~ 3.5 μm Ra. The substrates were then immersed in isopropanol solution followed by ultrasonication for 10 min, to remove any grit residue and contamination. All the coatings were deposited via atmospheric plasma spray process using an F4MB^{TM} (Oerlikon Metco, Westbury, NY, USA) spray torch. Each

coating architecture consisted of a 150-μm bondcoat layer of NiCoCrAlYHfSi (Amdry 386-2, Oerlikon Metco, Westbury, NY). The top coat for each coating contained four layers, TC1, TC2, TC3 and TC4. Each layer utilized an incremental mixture of NiCoCrAlYHfSi and yttria-stabilized zirconia (YSZ, SG 204, Saint Gobain Ceramics, Worcester, MA, USA). The details of each layer's metal/ceramic mixture and the associated processing conditions are shown in Fig. 1 and Table 1.

To understand thermal conductivity of each layer, specimens on each substrate material were prepared systematically with incremental top coat layers. The details of substrates and top coat layers on each specimen are summarized in Table 2.

A JEOL 8200X electron microprobe was used for high-accuracy elemental characterization of the coating. The EPMA provides qualitative (identification) and quantitative (composition) characterization for Be to U and also x-ray, secondary electron, backscatter electron and grain orientation imaging. Elemental x-ray maps were collected with five crystal-focusing spectrometers for wavelength dispersive x-ray spectroscopy (WDS). Quantitative line scans utilized a 15-kV accelerating voltage and an electron beam current of 100 nA. Certified elemental standards from Geller MicroAnalytical Laboratory, Inc. were used for determination of unknown elemental concentrations in samples analyzed for this study.

Thermal diffusivity of the coatings was measured using two flash diffusivity systems: a TA Instrument Flashline5000 and a Netzsch LFA 457 Microflash. The samples were 12.7 mm in diameter. Substrates were 1.5 mm thick, and the total coating thicknesses were from 0.2 mm to 0.9 mm. Standard thermal diffusivity testing following ASTM 1461-2009 was performed using classic analysis (Ref 13-16). Specific heat (C_p) was measured using a Netzsch 404C Pegasus differential scanning calorimeter
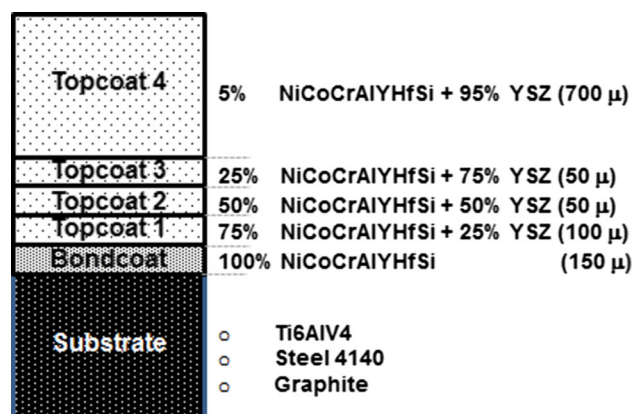

Fig. 1 Overall coating architecture used to prepare the thermal conductivity specimens

Table 1 Processing parameters used for bondcoat and top coat deposition

Material	Primary gas (Ar), slpm	Secondary gas (H$_2$), slpm	Carrier gas (Ar), slpm	Current (I), Amp	Spray distance, mm	Torch traverse speed, mm/sec	Powder feed rate, g/min
Bondcoat	47	6	4	550	100	500	30
Topcoat (TC1-4)	47	6	3	550	150	500	30

Table 2 Details of top coat layers deposited on the specimens

Specimen ID	Substrate	TC1 ($\sim$ 100 μm)	TC2 ($\sim$ 50 μm)	TC3 ($\sim$ 50 μm)	TC4 ($\sim$ 700 μm)	Total target coating thickness, μm
A	Ti-6Al-4 V					0
B	Ti-6Al-4 V	X	X	X		200
C	Ti-6Al-4 V	X	X	X	X	900
D	4140					0
E	4140	X	X	X		200
F	4140	X	X	X	X	900
G	Graphite	X				100
H	Graphite	X	X			150
I	Graphite	X	X	X		200
J	Graphite	X	X	X	X	900

Specimens A to F had 150-μm bondcoat layer

G–H were freestanding specimens after removing the graphite

(DSC) following ASTM 1269 (Ref 17) from room temperature to 800 °C at 20 °C/min heating and cooling rate in flowing Ti-gettered argon. Samples are about 5.5 mm in diameter. For thin samples, up to 4 disks were used to make the total mass between 130 and 150 mg and sapphire disks were used for the standard reference material. For all samples, thermal diffusivity (α), the average density (ρ) of the layers and C_p of the layered mixture were used to calculate thermal conductivity, κ:

$$\kappa = \alpha \rho C_p \tag{Eq 1}$$

Coatings sprayed on graphite spalled off due to thermal expansion mismatch during cooling after thermal spray, and the remaining graphite was ground off. Thus, samples G, H, I and J from Table 1 were used as freestanding coatings. Samples A, C and F were substrates and coatings on substrates.

As-deposited coatings were tested following conditions:

1. As-sprayed coating from room temperature to 800 °C
2. Anneal same samples in air at 800 °C for 100 h and repeat diffusivity tests

The maximum annealing temperature of 800 °C was selected to exceed the estimated maximum operating temperature of a typical Cummins diesel engine.

Results and Discussion

Microstructure Analysis

Figure 2(a) shows an SEM image of sample D with bondcoat on a 4140 steel substrate. The bondcoat showed a typical thermally sprayed microstructure with splats visible and an irregular substrate interface (due to grit blasting) and significant surface roughness. Since the major elements in the bondcoat and YSZ top coat are Ni and Zr, respectively, these elements were EPMA mapped and used to visualize distribution of these mixed metal and ceramic layers. As shown in Fig. 2(b), there is a clear interface between the substrate and bondcoat. Figure 2(c) shows averaged line scans of Ni and Zr across the coating thickness. The Ni distribution is uniform. Since there is no Zr present in bondcoat and no Ni in YSZ, Ni and Zr can be used to track the mixtures of bondcoat and YSZ. In sample E, in Fig. 3(a), a total of 200-μm-thick TC1, TC2 and TC3 were sprayed on top of the bondcoat. As indicated in Fig. 1, the wt.% of bondcoat changed from 75 to 50 and 25% and the wt.% of YSZ changed from 25 to 50 and 75%. The composition gradient is clearly shown in the EPMA Ni map Fig. 3(b) and Zr map Fig. 3(c). However, no interface between the bondcoat and TC1 is visible. The Monte Carlo

Fig. 2 (a) SEM image of sample D: bondcoat on 4140 Steel and (b) Element map for Ni (c) line scans of Ni and Zr
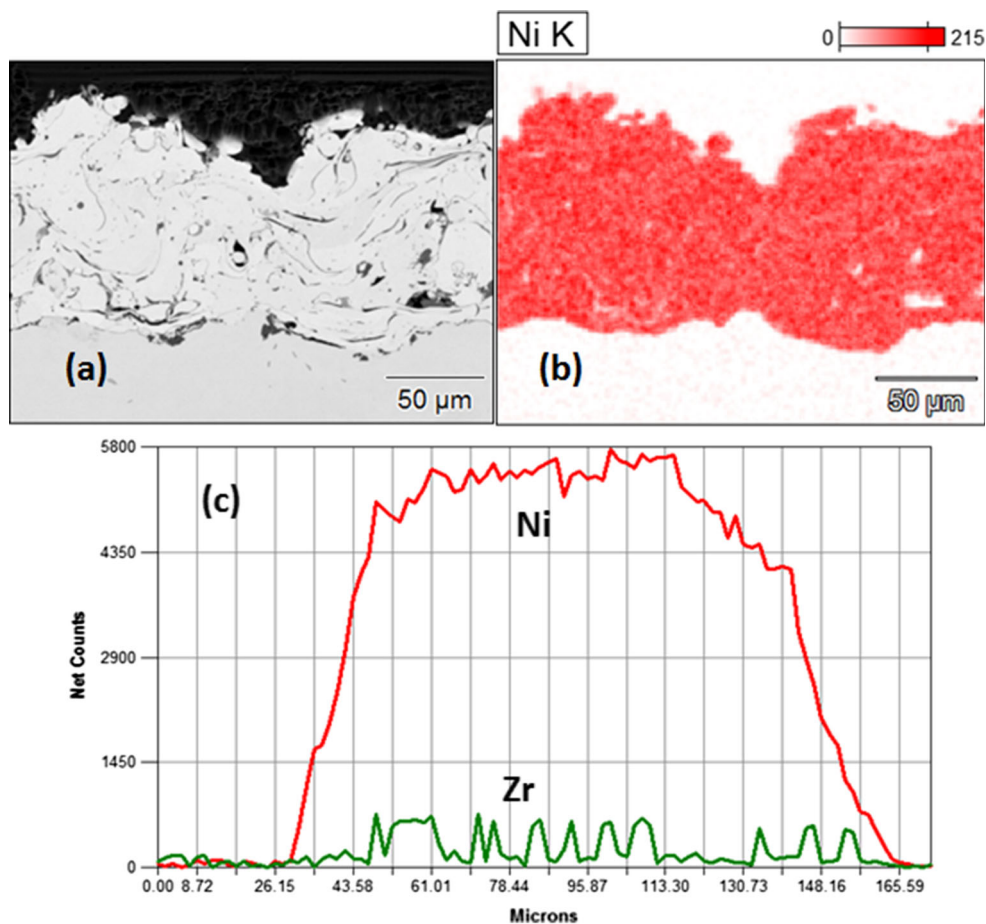
simulation of a 15 kV interaction volume in 3.7 g/cm^3 material shows z-depth of $\sim$ 650 nm and x–y spread of 1.2 microns. Fluorescence of x-rays can also occur as far as several microns away from the region of interest. These two factors combined to cause signal from YSZ elements (e.g., Zr) to be detected in the bondcoat region with no sharp transition. Figure 3(d) shows line scans of Ni and Zr from the steel substrate to the coatings. The transition from Ni to Zr occurred smoothly starting near 100 μm. The boundaries between TC1 and TC2, TC2 and TC3 were not present. This indicated a smooth transition from one layer to the next layer with the intended gradient of mixture.

The final coat, TC4, was 700 μm in thickness with 95% YSZ and 5% bondcoat. The SEM image in Fig. 4(a) shows the complete coating system F. The Ni and Zr maps in Fig. 4(b) and (c) show the distribution of each phase and transition from bondcoat to YSZ. The line scans in Fig. 4(d) show the Ni and Zr distribution throughout the coating. The transition area shows the selected 50 μm thickness and 25 wt.% change in mixture of each layer (TC1 to TC3) made the bondcoat to YSZ transition extend 200 μm. By changing the thickness and composition of each layer, it is possible to design the transition area to

reduce TBC thermal stresses on higher expansion substrates.

Thermal Transport Properties

Density of each freestanding TBC disk for diffusivity testing was measured from the weight and volume calculated from the thickness and diameter. The density of TBC G is 3.63 g/cm^3, TBC H is 3.74 g/cm^3, TBC I is 3.91 g/cm^3 and TBC J is 4.64 g/cm^3. The increasing trend is consistent with the increasing content of YSZ (6.10 g/cm^3). Specific heat of the samples G, H, I and J measured by DSC during heating is shown in Fig. 5(a). The four coatings all have bondcoat mixing with increasing amount of YSZ. Calculating specific heat using the rule-of-mixture could present large uncertainties due to the mass percentages of the bondcoat and YSZ in the actual coating are not measured. The results showed that C_p increases with more YSZ and the values of each coating increase with temperature. Coatings G, H and I all showed small step changes near 600 °C. Coating J, with more YZS, showed a barely detectable change. The change is likely a transition from glassy phase into crystalline phase of the bondcoat
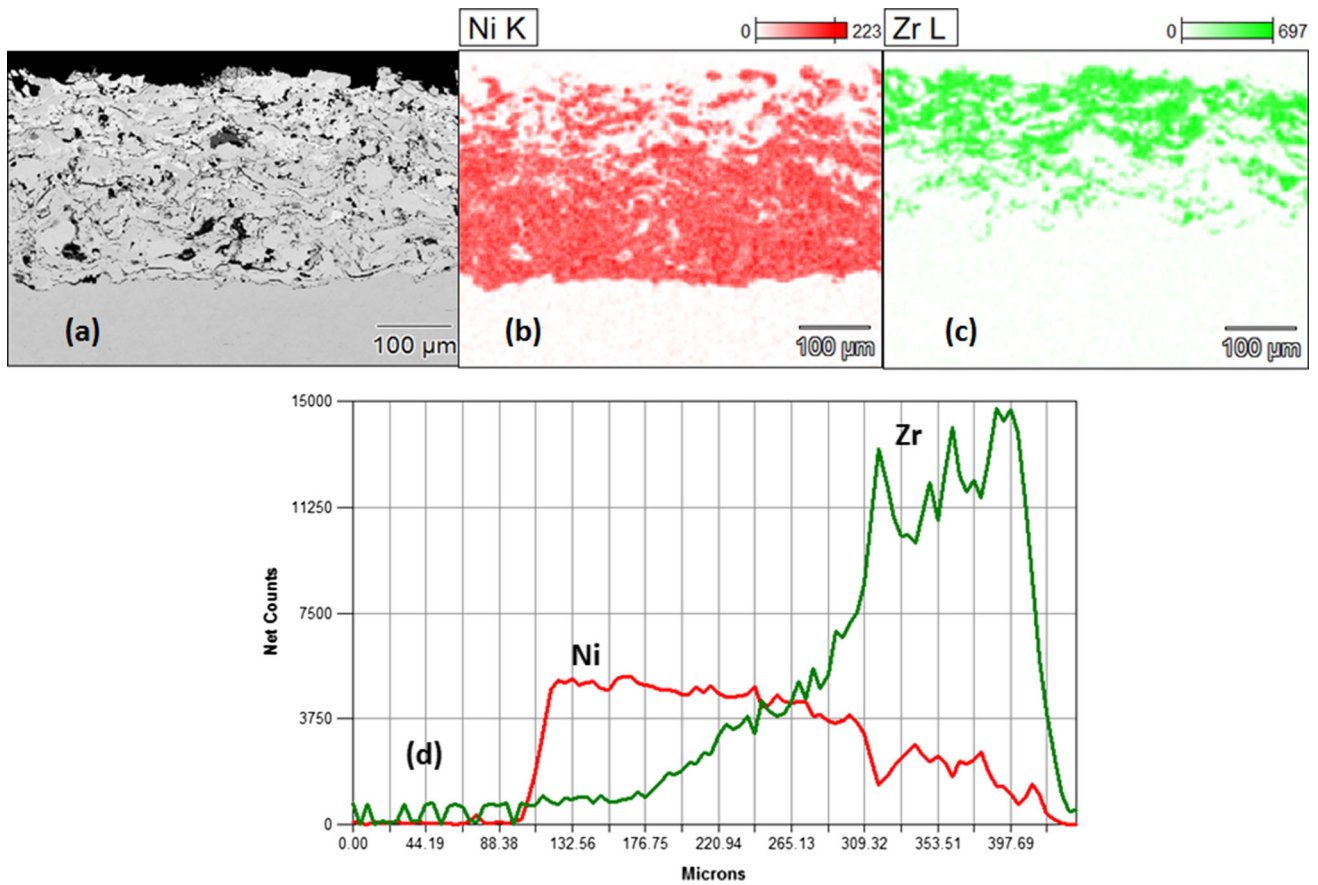
Fig. 3 Sample E:4140 Steel + Bondcoat + TC1 + TC2 +TC3 (a) SEM image of sample E, (b) EPMA element map of Ni, (c) EMPA map of Zr and (d) Line scans of Ni and Zr

alloy upon heating. It is possible for the as-sprayed layers to have residual amorphous contents upon cooling. This was mainly based on the broad "step-shaped" transitions in DSC signals and irreversible nature of these changes upon heating Fig. 5(a) and cooling Fig. 6(a). Additional high-temperature x-ray diffraction (XRD) is needed to confirm this. Figure 5(b) shows the thermal diffusivity of four as-sprayed freestanding coatings from room temperature to 800 °C. Coatings G, H and I are greatly influenced by the fraction of metallic bondcoat, and thermal diffusivity increased as a function of temperature. With increasing amounts of YSZ in H and I, the overall thermal diffusivity values decreased and the slope become less steep. In sample J, which has a 700 μm outer layer with 95 wt.% YSZ, thermal diffusivity is dominated by the ceramic and thus decreases as a function of temperature. At 500 °C, thermal diffusivity of samples G, H and J increased rapidly (indicated by a change in slope) and did not follow the heating curve during cooling. The increase in diffusivity after 500 °C and the hysteresis are an indication of grain growth in both the metal alloy and ceramic. However, sample J, which is mostly ceramic, did not show a change in slope, and only a small hysteresis was detectable. Only limited grain growth happened in the YSZ, and the increase in thermal diffusivity was too small relative to the changes in the other bondcoat dominating coatings. This is mainly due to the higher sintering temperature of the YSZ, usually above 800 °C. The measured C_p was used in thermal conductivity calculation as shown in Fig. 5(c). For a typical alloy, thermal conductivity is dominated by electronic contribution and increases as a function of temperature. For a typical ceramic, thermal conductivity is dominated by lattice vibrations (phonons) and decreases as a function of temperature.

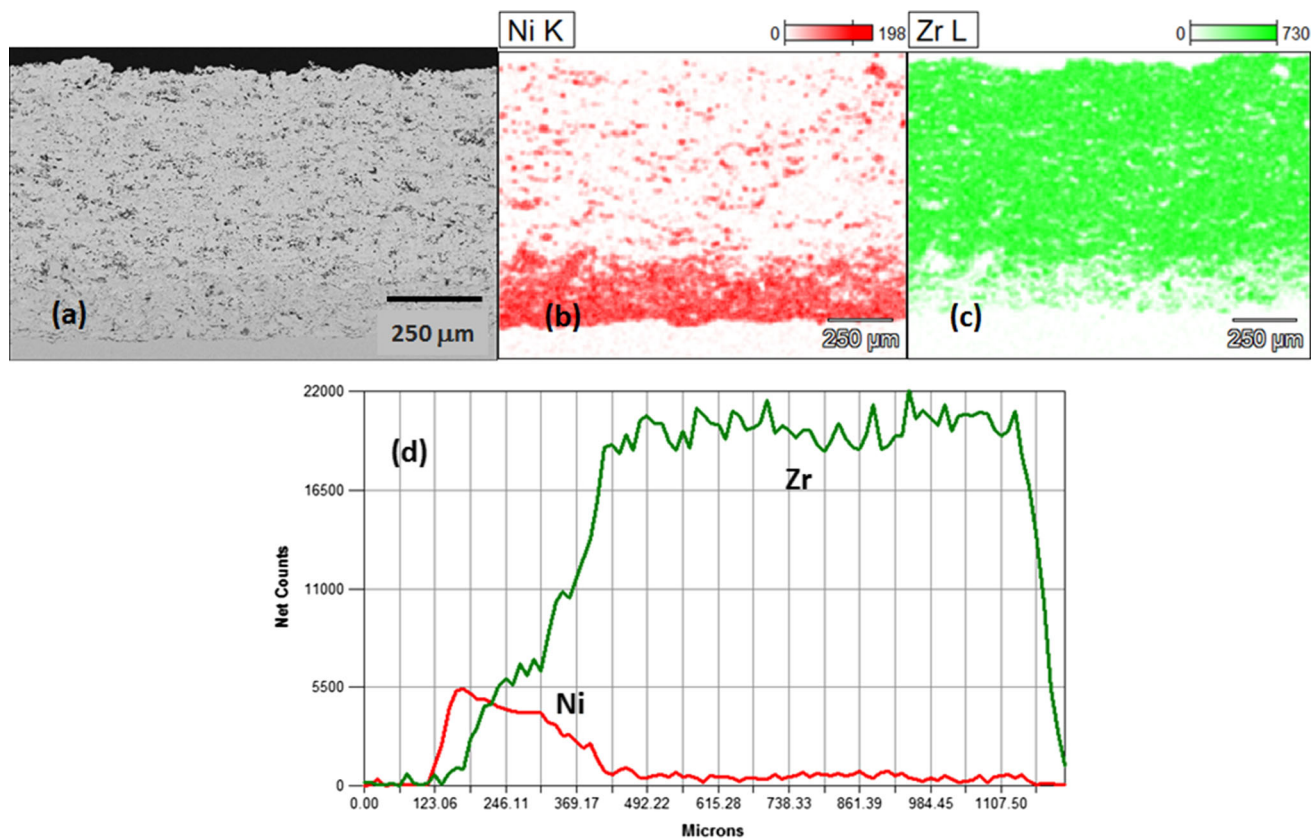A subsequent annealing was conducted on the four freestanding coatings in air at 800 °C for 100 h. Fig-

Fig. 4 Sample F: Bondcoat + TC1 + TC2 + TC3 + TC4 (a) SEM image of sample F, (b) EPMA element map of Ni, (c) EMPA map of Zr and (d) Line scans of Ni and Zr

ure 6(a) shows the specific heat of the coating during cooling. The step changes observed in heating were smaller indicating the possible transition is sensitive to thermal history. Thermal diffusivity was measured again and is shown in Fig. 6(b). Thermal diffusivity values at room temperature all increased significantly for sample G, H and I. Sample J did not show any increase in value after the measurements. Thermal diffusivities of samples G, H, and I all showed an increasing trend as a function of temperature. It is important to note that the hysteresis was eliminated after the annealing. Figure 6(c) shows the thermal conductivity calculated using C_p and density of the coating.

Two coatings with the full thickness of all layers, C and F, were tested with the Ti-6Al-4V and steel 4140 substrates, respectively. As shown in Fig. 7, the effective thermal diffusivities of the two coated samples (C and F) were lowered significantly by the TBCs and exposure at 800 °C did not show significant sintering and no hysteresis was detected after measurements at 800 °C. It should be noted that the thermal diffusivity values are only related to the 3-mm-thick substrate and the 900 µm TBC. A detailed two-layer analysis is needed to separate the TBC from the substrate. Since the freestanding TBCs have been

measured, this is used to demonstrate the effect of TBCs on two different substrates and the stability (no hysteresis).

Thermal conductivity of the graded TBC has room temperature values of 1.2 W/mK and decreases slightly at high temperatures. It is comparable to the TBCs based on YSZ (Ref 18). In fact, the mixing of 5 wt.% bondcoat with 95 wt.% YSZ in the final layer showed thermal conductivity was reduced by the additional alloy phase. The distribution of bondcoat (via Ni map) and YSZ (via Zr map) in Fig. 4(b) showed the additional interfaces of ceramic and bondcoat, and its graded distribution enhanced phonon scattering in the TBC. Oxidation is also possible for bondcoat material and exposure at high temperature in an YSZ matrix. Oxides, e.g., Al_2O_3, could be formed from MCrAlY (Ref 19). Due to the low operating temperatures of the diesel engine (< 650 °C), the oxidation process is expected to be slow and the amount of alumina formed to affect transport properties is limited. However, the long-term effect of MCrAlY/YSZ mixture needs to be studied. For this study, in addition to the intended thermal expansion match for better mechanical stability, thermal conductivity of the TBC did not increase due to the alloy contents.
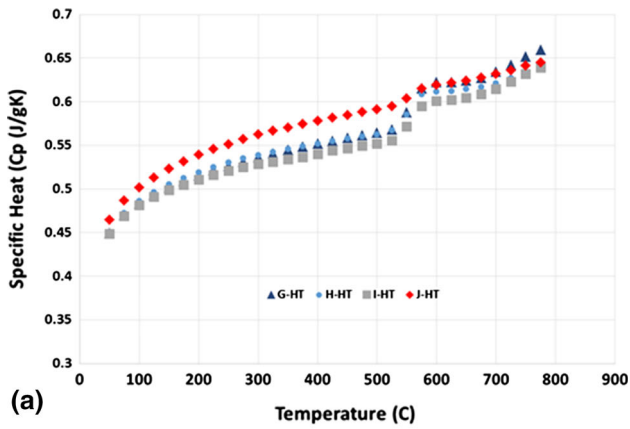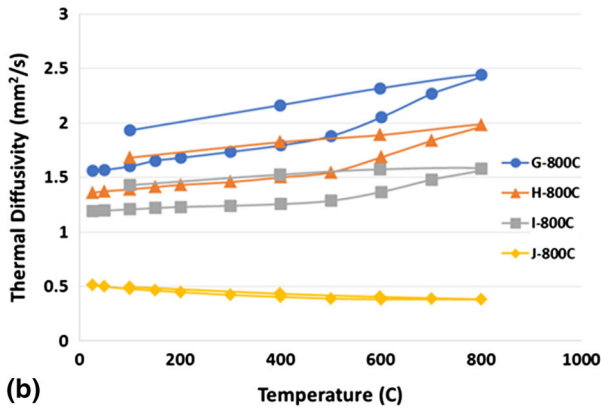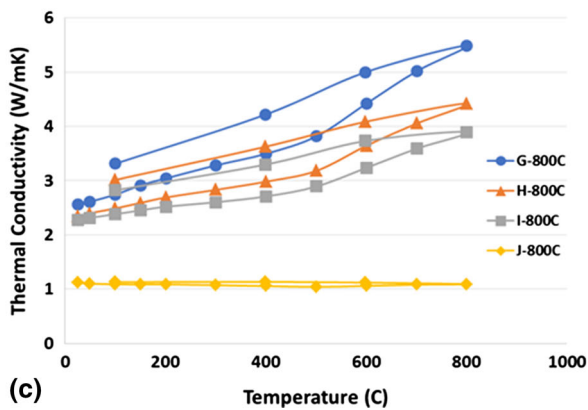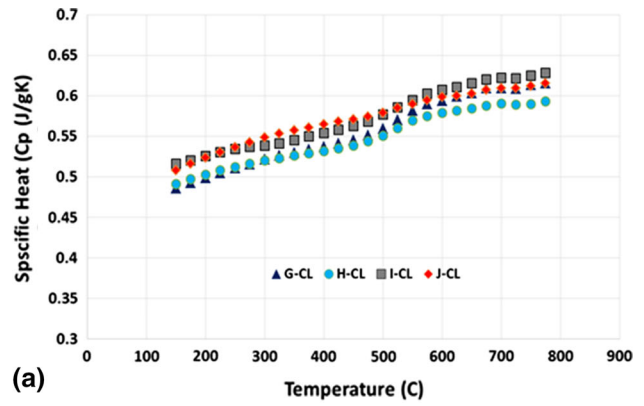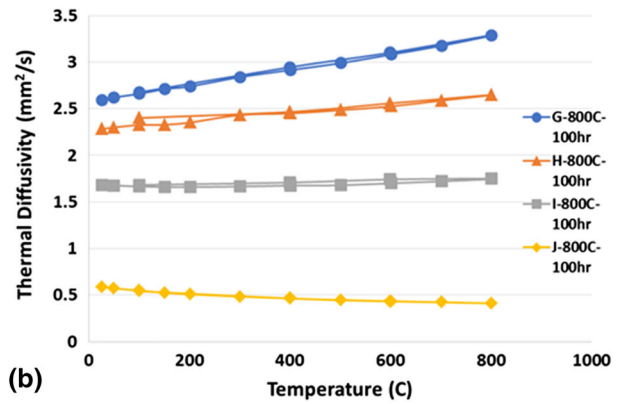
Fig. 5 (a) Specific heat, (b) thermal diffusivity and (c) thermal conductivity of coatings G, H, I, and J as a function of temperature. The lower lines in (b) and (c) for each coating represent data obtained during heating and the upper line represents data obtained during cooling the same specimen
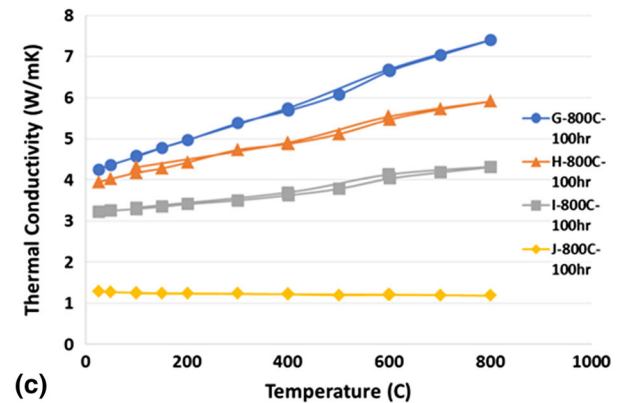

Fig. 6 (a) Specific heat, (b) thermal diffusivity and (c) thermal conductivity of samples G, H, I, J to 800 °C after aging at 800 °C

Summary

Graded TBCs with mixed layers of metallic bond coat and YSZ top coat were thermally sprayed. SEM and EPMA analysis showed the coatings achieved targeted thicknesses and provided the designed gradient. No distinct interfaces were observed among the various graded metal/ceramic layers, even though they were sprayed as discrete layers.

The smooth transition is anticipated to be beneficial to the thermal expansion matching and thermal stress accommodation. Thermal conductivity of the bondcoat dominated the multilayer coatings and showed behavior similar to metallic alloys with a large hysteresis upon high temperature exposure. The addition of 700-μm-top coat that was predominantly YSZ significantly lowered thermal conductivity and provided a systemic response with ceramic characteristics. The measured hysteresis behavior below 800 °C was suppressed by the thick outer layer of ceramic
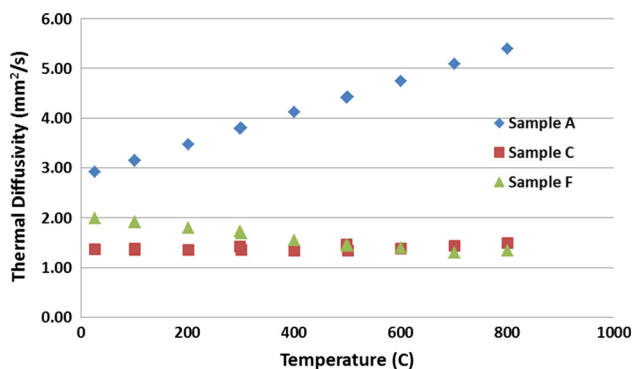
Fig. 7 Thermal diffusivity of sample A, C and F measured to 800 °C

coatings. The graded TBCs will be tested for mechanical durability and long-term thermal cycling.

References

1. R. Miller, *Surf. Coat. Technol.*, 1987, **30**(1), p 1-11
2. T. Hejwowski and A. Weronski, *Vacuum*, 2002, **65**(3–4), p 427-432
3. N.P. Padture, M. Gell, and E.H. Jordan, *Science*, 2002, **296**(5566), p 280-284
4. Y.J. Su, R.W. Trice, K.T. Faber, H. Wang, and W.D. Porter, *Oxid. Met.*, 2004, **61**(3–4), p 253-271
5. S.R. Choi, J.W. Hutchinson, and A.G. Evans, *Mech. Mater.*, 1999, **31**, p 431-447
6. T.M. Yonushonis, *J. Therm. Spray Technol.*, 1997, **6**(1), p 50-56
7. M. Azadi, M. Baloo, G.H. Farrahi, and S.M. Mirsalim, *Int. J. Automot. Eng.*, 2013, **3**(1), p 305-317
8. A. Levy and S. Macadam, *Surf. Coat. Technol.*, 1987, **30**, p 51-61
9. R. Tucker, What Should I Expect from Coating My Engine?, *Engine Professional*, 2010, Jan–Mar p 34-40.
10. S. Sampath, W.C. Smith, T.J. Jewett, and H. Kim, *Mater. Sci. Forum*, 1999, **308–311**, p 383-388
11. M.I. Mendelson, T.N. McKechnie, and L. B. Spiegel, in *Proceedings of the 18th Annual Conference on Composites and Advanced Ceramic Materials—A: Ceramic Engineering and Science Proceedings,* 2008, vol. 15, (4) p 555-562.
12. W. Chi, V. Srinivasan, A. Sharma, S. Sampath, and R. Gambino, in *Materials: Research Society Symposium Proceedings*, 2007, vol. 977 0977-FF04-15.
13. ASTM E 1461-13, *Standard Test Method for Thermal Diffusivity by the Flash Method*, ASTM, West Conshohocken, PA, 2013
14. W.J. Parker, R.J. Jenkins, C.P. Butler, and G.L. Abbott, *J. Appl. Phys.*, 1961, **32**, p 1679-1684
15. J.A. Cape and G.W. Lehman, *J. Appl. Phys.*, 1963, **34**, p 1909-1913
16. R.E. Taylor and L.M. Clark, III, *High Temp. High Press.*, 1974, **6**, p 65-72
17. ASTM E 1269-11, *Standard Test Method for Determining Specific Heat Capacity by Differential Scanning Calorimetry*, ASTM, West Conshohocken, PA, 2011
18. H. Wang, W.D. Porter, and R.B. Dinwiddie, *J. Therm. Spray Technol.*, 2010, **19**(5), p 879-883
19. F. Yang, X. Zhao, and P. Xiao, *J. Eur. Ceram. Soc.*, 2010, **30**(15), p 3111-3116